AIAA 80-0009R

Turbulent Trailing Vortices in Stratified Fluids

A. M. Hecht* and A. J. Bilanin*
Continuum Dynamics, Inc., Princeton, N. J.
and
J. E. Hirsh†
Aeronautical Research Associates of Princeton, Inc., Princeton, N. J.

The effects of stable atmospheric-density stratification, vortex core size, and turbulent scale on the descent of aircraft-trailing vortices are investigated using numerical solutions of a second-order closure turbulence model. A Boeing 747 vortex descent is simulated numerically and compared to reported measurements of descent distance, velocity, and circulation profiles. It is concluded that the pair was halted in its descent by a diffuse region of countersign vorticity primarily outboard and above the vortex cores. It is shown that the core size and turbulent macroscale have significant effects on vortex behavior through their influence on turbulence production, diffusion, and dissipation.

Nomenclature

Fr	= Froude number, $\Gamma_0/2\pi s^2 N$
g	= acceleration of gravity
N	= Brunt-Väisälä frequency, $[-(g/\rho_0)\mathrm{d}\rho_0/\mathrm{d}z]^{1/2}$, $[(g/\theta_0)\mathrm{d}\theta_0/\mathrm{d}z]^{1/2}$
P	= impulse
q	= root mean square of twice the turbulent kinetic energy
r	= radial coordinate measured from center of vortex-pair core
r_1	= radius of maximum swirl velocity
s	= vortex-pair semiseparation distance
T	= kinetic energy
t	= time
u,v,w	= velocities parallel to x, y, and z coordinates, respectively
V	= vortex-pair descent velocity
w	= core swirl velocity
x,y,z	= coordinates parallel to vortex-pair cores, horizontal and vertical, respectively
Γ	= vortex-pair circulation
ϵ	= dissipation rate, $(1/8)(q^3/\Lambda)$
ζ	= vorticity
θ	= mean temperature
Λ	= turbulent macroscale parameter
ν	= kinematic viscosity
ρ	= density
σ	= core vorticity spread parameter
ψ	= stream function

Subscripts

avg	= average
c	= countersign
max	= maximum value
p	= principal vortex
0	= initial value

Superscripts

$(\bar{\ })$	= ensemble averaged
$(\ )'$	= deviation of variable from its initial condition

Presented as Paper 80-0009 at the AIAA 18th Aerospace Sciences Meeting, Pasadena,Calif., Jan. 14-16, 1980; submitted Jan. 16, 1980; revision received Jan. 5, 1981.

*Senior Associate. Member AIAA.
†Associate Consultant. Member AIAA.

I. Introduction

TRAILING vortex wakes of wide-body transports are a significant threat to following aircraft due to the considerable rolling moments they generate. The safety hazard they impose and the economic impact created by increased aircraft separation requirements during takeoff and landing have spurred numerous analytical and experimental studies of vortex behavior. Simplifying assumptions which have been adopted to achieve purely analytical solutions have resulted in contradictory predictions of vortex descent in the real atmosphere.[1-10] Numerical methods must be used to more fully account for real fluid effects, such as turbulence. The present investigation has been carried out to clarify the effects of stratification on aircraft vortex descent. The calculations reported here were made with WAKE, a finite difference computer code which solves the two-dimensional, unsteady mean and ensemble-averaged Reynolds stress equations of fluid motion based on a second-order closure turbulence model. The axisymmetric version of the WAKE code was used, as reported by Hecht et al.,[11] to validate the model for vortex flows in stratification by numerically simulating the measured descent of vortex rings in discontinuous and linear-density stratified fluids. The agreement between the calculated and measured vortex-ring trajectories and geometric parameters provided the necessary validation of the model for stratified fluids and opened the way for the study of a full-scale flight-test vortex-pair descent.

The flight data analyzed here were selected from a set of measurements reported by Burnham et al.[12] which consist of Boeing 747 vortex-pair rotational velocity, descent velocity and altitude and inferred circulation profile histories. The numerical simulation was run using an initial vortex rotational velocity close to the actual initial data. The measured core spread was small compared to the size of the computational domain normally required to define the flow in and adjacent to the recirculation cell, and the maximum rotational velocity was exceptionally high. The size of the numerical grid required to resolve the core flow, combined with the large velocities in this region, lead to a very small allowable time step to preserve numerical stability. A new method was devised to calculate the evolution of tight, strong vortices based on computing the departure of the vortex from an analytically defined initial condition. For the vortex pair analyzed, this departure remained small during most of descent.

Results of the code were used as a guide in interpreting vortex-pair behavior in a stratified atmosphere, and the role of turbulence in influencing this behavior.

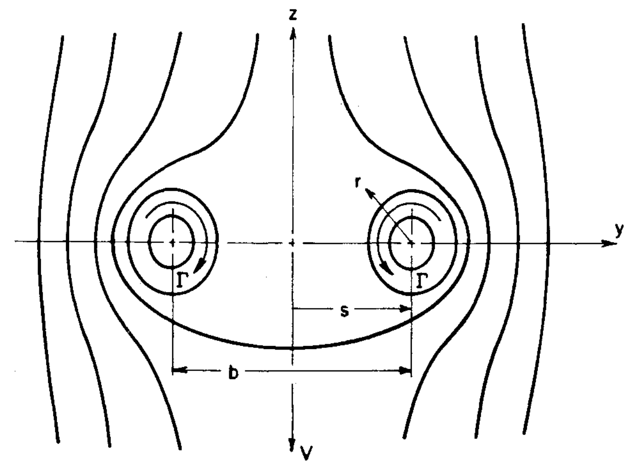

Fig. 1 Vortex pair coordinates and parameters.

Past analytical and numerical treatments of vortex wakes in the stratified atmosphere provide no clear consensus regarding vortex spacing, descent velocity and the effect of buoyancy generated vorticity. The descent velocity of a vortex pair with concentrated vorticity in a uniform density field is

$$V=(\Gamma/4\pi s)+O(\sigma/s)^2 \tag{1}$$

where s is core semiseparation and σ the core radius. Out of ground effect, vortices exhibit a remarkable persistence. The highly stabilizing rotational motion in the core suppresses the production of turbulence,[13] significantly reducing the rate of radial diffusion of core vorticity. Vortex lifetime appears to be limited mainly by ambient turbulence effects[13] and three-dimensional instabilities.[14] In the presence of ambient cross shear, the lifetime of one vortex of the pair may actually be enhanced due to the dissipation of the other vortex by shear.[15]

Vortex-pair descent in a stably stratified fluid results in a complex flow pattern of fluid having nonuniform density. A recirculation cell with density $\rho(y,z,t)$ penetrates heavier ambient fluid of density $\rho_0(z)$ (see Fig. 1). Production of vorticity occurs locally at a rate proportional to $\partial\rho/\partial y$. The behavior of the vortices is intimately tied to the generation, convection, and diffusion of this vorticity. The difference in the various theories which have been proposed to predict stratification effects are basically in how these processes are modeled, resulting in contradictory predictions of vortex separation and descent history. Theoretical approaches have led mainly to two types of predicted behavior during descent: vertical deceleration with increased separation and acceleration with decreasing separation. Observed behavior during full-scale flight experiments have indicated deceleration of the vortices,[12,15] although the exact role of stratification in this effect has been ambiguous.[15]

Space does not permit a thorough review of previous analytical treatments of the problem. For a brief description of past approaches, see Hecht et al.[16] Comparisons between selected analytical theories and the present numerical calculations will be presented later in this paper.

II. The WAKE Computer Code

The WAKE code is a two-dimensional unsteady, incompressible flow computer program developed to simulate the dynamics of multiple aircraft vortices in a turbulent-stratified atmosphere. It solves the equations of Donaldson's second-order closure model of turbulent transport.[17] A second-order model implies that the partial differential equations are solved for the Reynolds stress tensor $\overline{u_i u_j}$ as well as for the mean ensemble-averaged variables. Higher order unknowns and certain second-order correlations in the Reynolds stress equations have been replaced by modeled terms containing constants and second-order correlations. A derivation of the modeled Reynolds stress equations for the second-order turbulence correlations and a discussion of the model development and constant evaluation may be found in Lewellen and Teske.[18] A complete description of the code as it was used in the present study can be found in Hecht et al.,[16] including the equations of mean motion and the modeled equations for the ensemble averaged turbulence correlations.

Table 1 Flight parameters and meteorological factors of run 8, 1975, Rosamond dry lake tests[12]

Flight time	0745 PST
Altitude	244 m
Airspeed	77 m/s
Aircraft weight	244,000 kg
Flap setting	30/30 (deg)
Landing gear	Down
Spoilers	None
Thrust (EPR)	1.20
Wind speed	1 m/s
Wind direction	310 deg
Atmospheric dissipation rate ($\epsilon^{1/3}$)[a]	1.4 cm$^{2/3}$/s
Lapse rate	1°C/100 m
Flight attitude	Level

[a] At flight altitude.

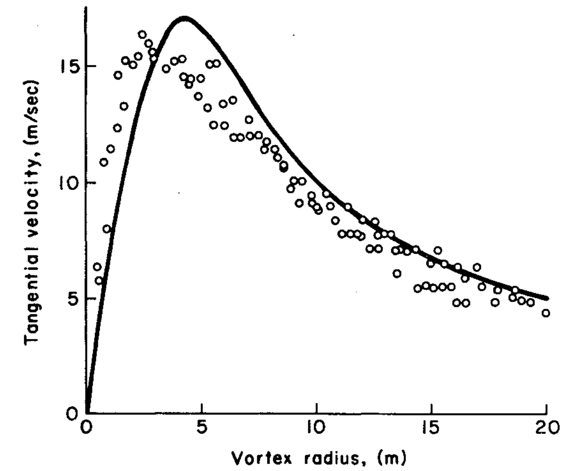

Fig. 2 Measured swirl velocity vs radius and analytical profile based on a Gaussian vorticity distribution at 11 s.

III. Comparison of WAKE Calculations with Full Scale Flight Data

Data Selection

To reduce extraneous effects which cannot be included in a numerical calculation, certain criteria were established as a guide in selecting an experimental test case. A measurement made on a clean aircraft configuration (minimum flaps, no spoilers) in level flight, out-of-ground effect, and in stable atmospheric stratification was sought. Calm ambient conditions, e.g., low cross shear and ambient turbulence, were factors considered. The number and quality of measurements made during the test were also major factors in selection.

The measurement selected for numerical simulation was run 8 of the 1975 Rosamond Dry Lake tests, made using a Boeing 747 aircraft. A complete description of these tests and data for all runs have been reported by Burnham et al.[12] Measurements of vortex characteristics were taken with the aircraft in a variety of flap settings, landing gear, and spoiler configurations and meteorological conditions. Takeoff, level flight, and landing aircraft altitudes also were varied. A total of 54 passes were flown at altitudes varying from 30 to 244 m. Length of computation time prevented analysis of more than one of these passes, despite reductions due to the improved numerical technique.

Test Conditions

The important flight and environmental parameters for the selected test are given in Table 1. The total circulation generated by the aircraft during run 8 was reported to be 628 m^2/s, the initial vortex separation to be 50 m, and the initial descent rate to be 2 m/s. A total of about 80 s of test time was recorded.

The measured swirl velocity profile at 11 s after passage of the generating aircraft is shown in Fig. 2. Also shown is the analytical swirl velocity derivable from the approximate initial vorticity distribution used in the WAKE calculation. A Gaussian vorticity distribution was used to approximate the initial condition, with peak vorticity and spread chosen to match the velocity profile as closely as possible.

The stable ambient stratification at the flight altitude was measured to be 1°C/100 m. During descent, however, a vortex pair compresses at a rate of approximately 1°C/100 m if the compression is adiabatic. The calculations were performed using potential temperature and the stratification was set equal to 2°C/100 m. The effective Brunt-Väisälä frequency was therefore

$$N=\left[\frac{g}{\theta_0}\frac{\mathrm{d}\theta_0}{\mathrm{d}z}\right]^{1/2}=0.0265\ \mathrm{rad/s} \tag{2}$$

where $\theta_0 = 280°C$. Defining the Froude number to be

$$Fr=\frac{\Gamma_0}{2\pi s_0^2 N} \tag{3}$$

the Froude number for run 8 at 11 s after aircraft passage was equal to 6.0.

The initial turbulence level generated by the pair was estimated by observing the time required for entrained smoke to diffuse throughout the recirculation cell, giving $q^2 \cong 1$ m^2/s^2. The approximate ambient turbulence level was derived from the measured dissipation rate ϵ, leading to an ambient turbulence value of ~ 0.03 m^2/s^2 (based on an assumed ambient turbulence scale of 2.5 m), a level which is negligible in its effect on the vortex descent on the time scale of the stratification effect.

The macroscale Λ of the self-generated turbulence is one of the most uncertain variables of vortex-flow phenomena in the atmosphere. It is expected that this scale may be controlled by the characteristic dimensions of the flowfield, which in this case are the core radius, the core separation, and the length associated with the gradient of density occurring at the boundary of the cell of recirculating fluid. Generation of the turbulence and the length scale of this turbulence is a function of the core size and the density gradient scale in the respective regions of turbulence production. Guided by the results of Ref. 11, where it was found that a macroscale equal to 3% of the initial vortex-ring radius produced the best simulation of data, we set $\Lambda = 0.03$ s for the present calculation. A brief sensitivity study of macroscale effects on vortex descent in stratification is presented in Sec. IV.

Numerical Technique for Strong Vortices

The swirl velocity profile shown in Fig. 2 represents a wake having large-vorticity gradients. To resolve the tight, high velocity core numerically as well as the sharp density gradient at the edge of the recirculation cell requires a certain minimum numerical grid density and a sufficiently small time step for accuracy and stability. The domain must also be sufficiently large to avoid wave reflections at the boundaries from interfering with the calculation. Calculating the flow in the normal fashion by specifying the initial vorticity field in a highly dense mesh over a large domain would require a prohibitively large, high-speed computer. A new procedure was therefore devised to calculate vortex evolution by exploiting the slow decay characteristics of strong vortex flows. The vorticity was split into the sum of its analytically defined initial condition and its time- and space-dependent departure from that condition. The equation defining the deviation of the vortex from its initial condition becomes

$$\begin{aligned}\frac{\partial\zeta'}{\partial t}+(v_0+v')\frac{\partial\zeta'}{\partial y}+(w_0+w')\frac{\partial\zeta'}{\partial z}\\=-(v_0+v')\frac{\partial\zeta_0}{\partial y}-(w_0+w')\frac{\partial\zeta_0}{\partial z}-\frac{g}{\theta_0}\frac{\partial\theta}{\partial y}\\-\frac{\partial^2}{\partial y\partial z}(\overline{vv}-\overline{ww})+\left(\frac{\partial^2}{\partial y^2}-\frac{\partial^2}{\partial z^2}\right)\overline{vw}+\nu\nabla^2(\zeta_0+\zeta')\end{aligned} \tag{4}$$

where the zero subscript denotes variables associated with the analytically derived initial vorticity field. The deviation from this condition is denoted by primes. The deviation of the stream function from its initial condition is

$$\nabla^2\psi'=-\zeta' \tag{5}$$

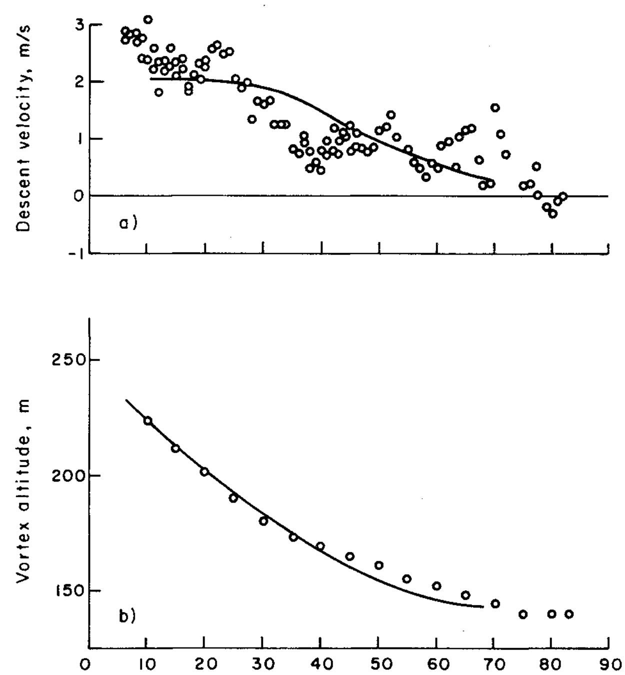

Fig. 3 Comparison between measured and calculated vortex descent velocity a) and altitude b) and time.

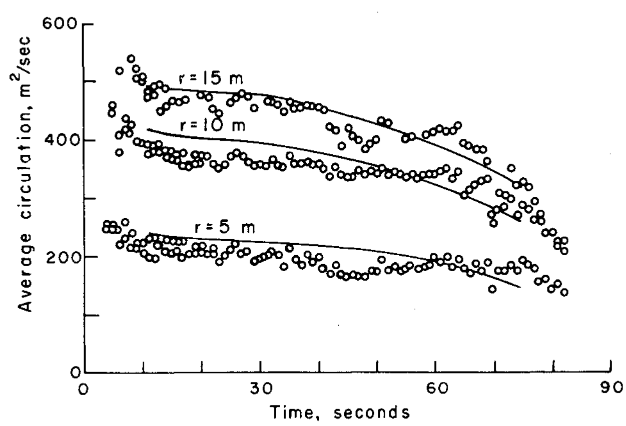

Fig. 4 Comparison between measured and calculated average circulation vs time at 5, 10, and 15 m radius from vortex center.

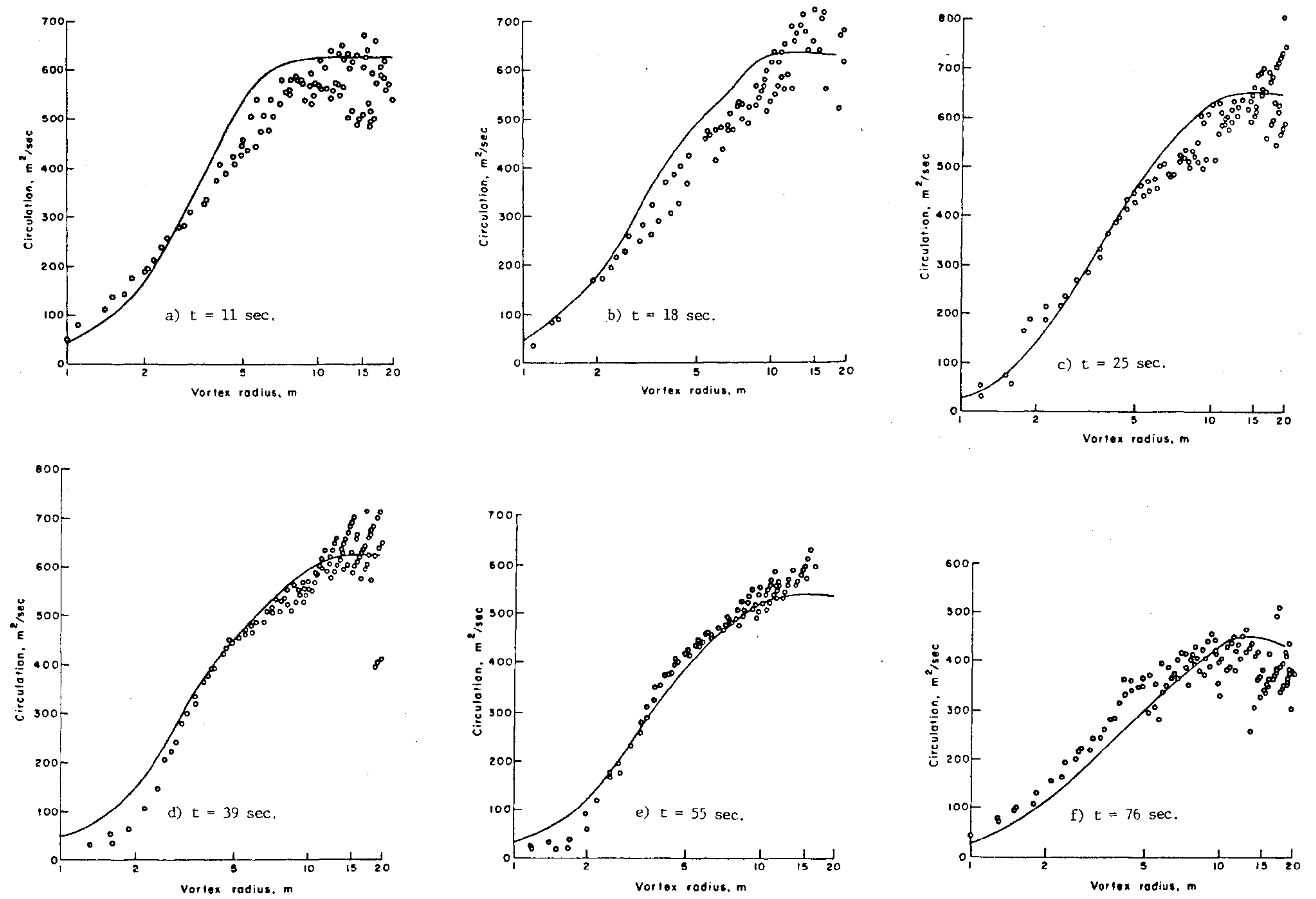

Fig. 5 Comparison between the measured and calculated circulation during descent.

and

$$v' = -\frac{\partial \psi'}{\partial z} \tag{6a}$$

$$w' = \frac{\partial \psi'}{\partial y} \tag{6b}$$

The vortices are kept in the center of the computational domain by an algorithm which traces the maximum total vorticity $\zeta = \zeta_0 + \zeta'$ and by adding the appropriate vertical washing velocity into the calculation. This technique reduced the numerical gradients over most of the vortex lifetime, leading to a reduced grid spacing requirement and consequently a larger allowable time step.

To provide a smooth generating function for the initial vorticity, a Gaussian profile (Lamb vortex) was chosen to match the swirl velocity and circulation profiles as closely as possible with this type of distribution. The vorticity used for the calculations was

$$\zeta_0 = \frac{\Gamma_0}{\pi\sigma^2}\left[e^{-(r_+/\sigma)^2} - e^{-(r_-/\sigma)^2}\right] \tag{7}$$

r_+ is measured from the center of the vortex located at $y = 25$ m, $z = 0$ m and r_- from $y = -25$ m, $z = 0$ m. σ is the spread of the core vorticity, equal to 3.7 m, and the maximum vorticity, $\Gamma_0/\pi\sigma^2$, is 14.4/s. These values correspond to the vorticity distribution which produces the analytical velocity profile in Fig. 2. Sensitivity of the results to the initial vorticity distribution could not be evaluated because of the large calculation time for even one run.

The perturbation and initial velocities enter the calculation of the turbulence correlations in the advection terms and the velocity gradient terms (see Ref. 16 or 19). The advection terms in the Reynolds stress equations were treated as shown above for the vorticity equation. The velocity gradients in the production terms of the turbulence equations were written as the sum of the analytically derived gradients of the initial velocity and the numerically calculated gradients of the perturbation velocities.

Comparison of WAKE Calculations With Data

The data reported by Burnham et al. in Ref. 12 included histories of the vortex-pair descent velocity and altitude, separation between vortices, maximum tangential velocity, and the vortex circulation and average circulation vs radius. This last was defined in Ref. 12 as

$$\Gamma_{\text{avg}} = \frac{1}{r}\int_0^r \Gamma(r)\,\mathrm{d}r \tag{8}$$

The calculation vortex-pair descent velocity and altitude are compared with the measured values in Figs. 3a and 3b, respectively. The measured descent velocity and vortex altitude oscillate about a mean which is represented by the calculated values. These oscillations persist far longer than any influence from secondary vortices might be expected to last, and are presently unexplained. Note that both the measured and calculated tip-vortex descent velocities decrease monotonically and do not accelerate.

Figure 4 shows a comparison between the measured and calculated average circulation, defined by Eq. (8), at 5, 10, and 15 m radii from the center of the core. Γ_{avg} was calculated using a radially varying $\Gamma(r)$, which in turn was an area integration of the vorticity out to a maximum radius defined by the distance from the center of the core to the centerline between the vortices.

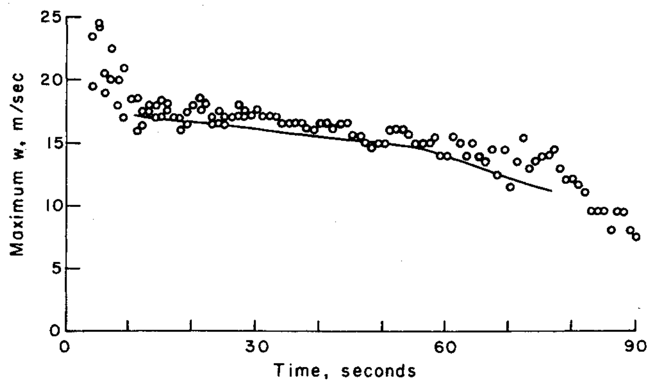

Fig. 6 Comparison between measured and calculated maximum swirl velocity history.

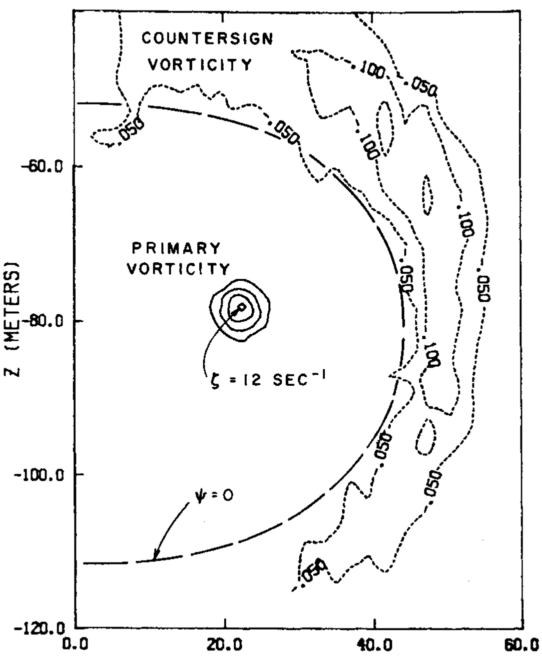

Fig. 7 Contours of primary and countersign vorticity at 65 s. Contour intervals: primary vorticity (———), 3.0/s; countersign vorticity (------), 0.05/s.

The measured and calculated profiles of circulation, $\Gamma(r)$ vs r, from 11 to 76 s after generation are presented in Figs. 5a-5f. The characteristics of the measured circulation and average circulation profiles are well represented by the calculations. The initial rate of decrease in Γ and Γ_{avg} is small, increasing gradually to the end of the measurement. The decrease in circulation with radius as the edge of the recirculation cell is approached is due to the countersign vorticity in this region. This decrease is predicted by the calculation, and can be seen in the data.

Figure 6 shows a comparison between maximum-tangential velocity and the calculated value. Again, the agreement is excellent over most of the data period. Note that, even after the vortex pair has stopped descending, there is still an appreciable swirl velocity in the core. The vortices, therefore, have considerable strength remaining although they have been stopped in their descent by the stratification, confirming the result found previously in Ref. 11.

One of the vortices drifted beyond instrumentation range at about 20 s and vortex separation could not be measured beyond that time. The calculated separation remained nearly constant during most of descent, decreasing gradually after 60 s to about 80% of the initial value. This is more than previously calculated using second-order closure for vortices in stratification.[11]

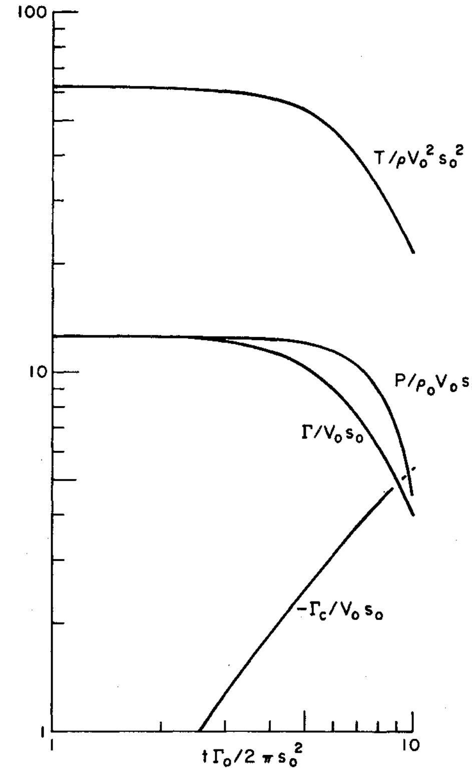

Fig. 8 Calculated nondimensional kinetic energy, impulse, total circulation, and integrated countersign vorticity.

The core vorticity calculation showed a slow decay over most of the test period. Figure 7 shows contours of the calculated vorticity in the core region at 65 s with contour intervals of 3/s. Although small in value locally, the large extent of the countersign vorticity is sufficient to stop the descent of the primary vorticity in and around the cores.

The balance between the calculated primary and countersign vorticity can be appreciated by seeing their variation with time, Fig. 8, which is plotted nondimensionally (time zero corresponding to 11 s after aircraft passage). The total circulation Γ decreases by nearly 50%, a consequence of the countersign circulation Γ_c. Circulation of the primary vortex $\Gamma_p = \Gamma - \Gamma_c$, however, remains high. Note that Γ_c is nearly linear in time for this vortex. Also shown in Fig. 8 are T, the total kinetic energy of both vortices, which initially is approximately equal to that of an elliptically loaded wing, and P, the impulse. There appears to be no simple time dependence for either the impulse or the kinetic energy.

The calculated streamline patterns at 11, 39, 55, and 65 s are shown in Figs. 9a-9d, respectively, in vortex-fixed coordinates. The recirculation cell area decreases gradually only near the end of descent, again in agreement with findings previously reported.[11]

The calculated turbulence intensity q^2 exhibited a maximum in a ring of approximately 6 m radius, decreasing to 10% of this maximum at the core center. The turbulence field remains remarkably constant with time due to the very tight, stable core structure. The maximum velocity associated with the turbulence is approximately 10% of the maximum swirl velocity. Note that a simpler turbulence model, for instance, a two-equation model, would not be adequate to predict the stabilizing effect of the rotational core which suppresses q^2 in this region. Lack of such suppression would lead to vortex dissipation at a more rapid rate than predicted here.

No temperature measurements were made for the tests analyzed here. Most notable about the calculated temperature field was the uniformity of temperature throughout the recirculation cell. The potential temperature of the cell remained very nearly at the initial value, indicating only slight

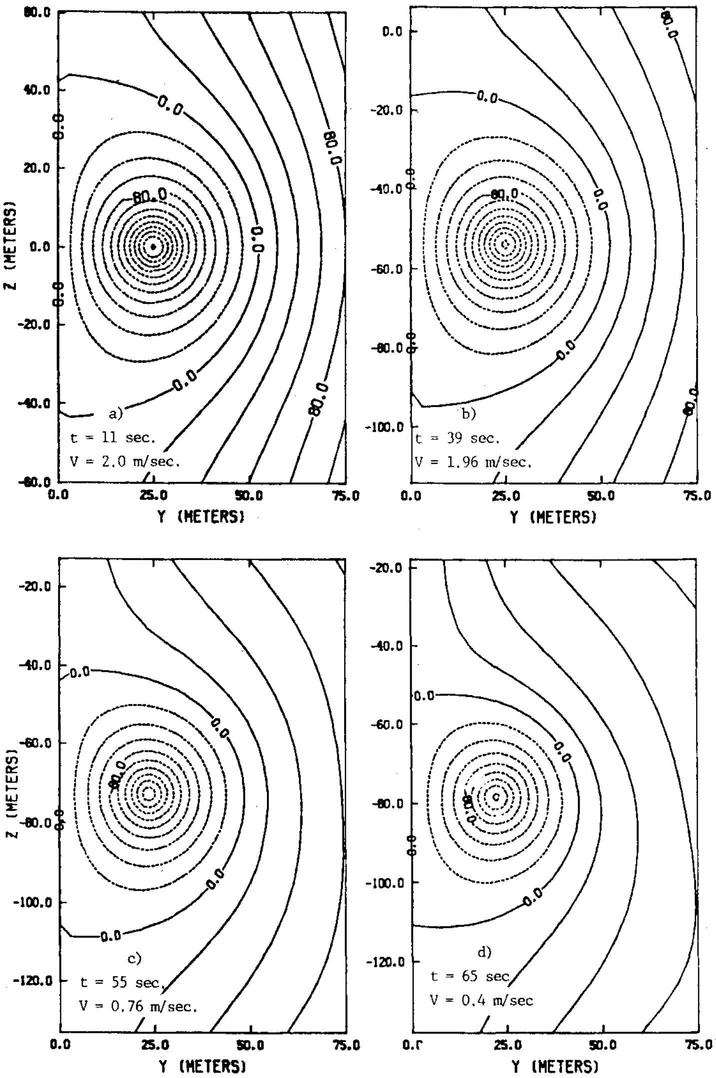

Fig. 9 Streamlines of descending recirculation cell at 11, 39, 55, and 65 s. Contour interval of 20 m^2/s.

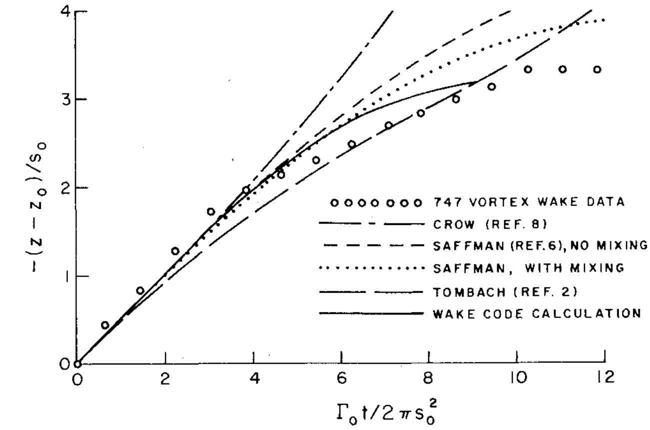

Fig. 10 Comparison of measured 747 vortex-wake descent trajectory with WAKE code result and several representative predictions for $Fr = 6.0$.

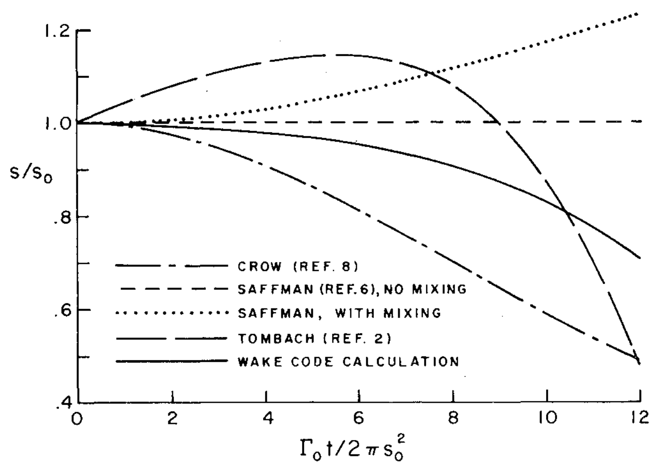

Fig. 11 Calculated-vortex semiseparation of the WAKE code and several analytical predictions for $Fr = 6.0$.

entrainment of ambient fluid during descent. The potential energy of the cell is therefore primarily a function of the cell area and the descent distance.

The descent and vortex separation predicted by several representative theories for these vortices are shown in Figs. 10 and 11. The analytical descent predictions are compared with the WAKE code calculation and with the Boeing 747 measurements. The Crow result plotted in these figures does not include the upwash vorticity. Saffman's prediction including mixing was calculated using a value of entrainment parameter α equal to 0.1. Tombach's prediction was calculated for a scale parameter of his analysis $s = 10.0$ (in Tombach's notation).

IV. Influence of Core Size and Turbulent Macroscale

The initial-energy content of a vortex pair per unit length of wake may be expressed as

$$T_0 = (\pi/8)\beta\rho_0\Gamma_0^2 \tag{9}$$

where β is defined as the ratio of the initial kinetic energy to the energy of a pair generated by an elliptically loaded wing. Since elliptic loading corresponds to minimum induced drag, $\beta \geq 1$. For a Gaussian vorticity profile, β is a function only of σ/s_0, see Table 2.

If it is assumed that the area of the recirculation cell remains constant and no entrainment or detrainment of fluid occurs, a maximum theoretical descent can be derived by equating the initial kinetic energy, Eq. (9), to the final potential energy of the cell at the end of descent. This was done in Ref. 11 and the result was shown to be

$$z^*_{max}/s_0 = -1.65\beta^{1/2}Fr \tag{10}$$

where the asterisk designates this as the theoretical result. A comparison of the nondimensional initial kinetic energy, maximum swirl velocity, radius of maximum swirl velocity, and z^*_{max} for $Fr = 6.0$ is shown in Table 2 for various values of the initial core spread parameter σ/s_0. Note that core size ratios greater than about 0.18 represent initially dissipated and diffused wakes.

Figure 12 is a comparison of calculated descent for two different initial-core sizes with $\Lambda/s_0 = 0.03$. The calculated separation for these core sizes agreed to within 5%.

The descent trajectory shown in Fig. 12 illustrates that the behavior of the pair is more complex than might have been anticipated from Eq. (10), which predicts increasing maximum descent for increasing initial energy. The maximum descent of a pair with $\sigma/s_0 = 0.5$ is predicted to be greater than that of a pair with $\sigma/s_0 = 0.15$, where $\Lambda/s_0 = 0.3$ and $Fr = 6.0$ for both. The initial kinetic energy of the latter is almost twice that of the former. The predicted vortex-pair separation (not shown) is nearly identical for both cases.

The effect of turbulence macroscale on the descent of initially aged vortices is shown in Figs. 13 and 14 for $Fr = 6.0$.

Table 2 Effect of core size on a pair of Gaussian (Lamb) vortices

$\frac{\sigma}{s_0}$	β	$\frac{T_0}{\rho_0 V_0^2 s_0^2}$	$\frac{2\pi s_0 w_{\max_0}}{\Gamma_0}$	$\frac{r_{I_0}}{s_0}$	$\left(\frac{z^*_{\max}}{s_0}\right)_{Fr=6.0}$
0.15	1.06	65.8	4.25	0.17	−10.19
0.30	0.74	45.9	2.13	0.34	− 8.52
0.50	0.55	33.8	1.28	0.56	− 7.34

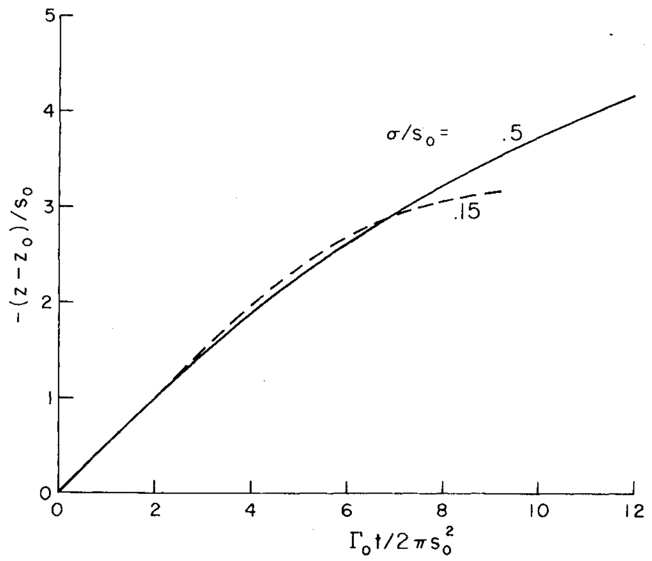

Fig. 12 Calculated wake descent for $\sigma/s_0 = 0.15$ and 0.5 for $\Lambda/s_0 = 0.03$, and $Fr = 6.0$.

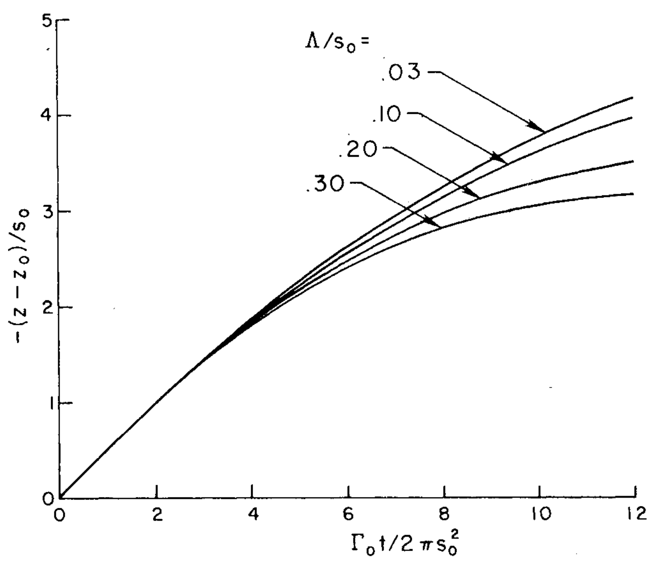

Fig. 13 Calculated descent trajectory for four values of the turbulent scale and $\sigma/s_0 = 0.5$ and $Fr = 6.0$.

The results show the calculated descent and separation for $\sigma/s_0 = 0.5$ and $\Lambda/s_0 = 0.03$, 0.1, 0.2, and 0.3. The maximum descent decreases with increasing scale while separation decreases monotonically for $\Lambda/s_0 = 0.03$ and 0.1, but initially increases before starting to decrease for scale ratios of 0.2 and 0.3.

By examining a limiting case of turbulent-shear flow in a Lamb vortex, Donaldson and Bilanin[13] showed that $q_{\max}/V_0$ is proportional to Λ/σ. This result was based on a "superequilibrium" theory of turbulence, developed on the assumption that at each point in the flow the turbulent

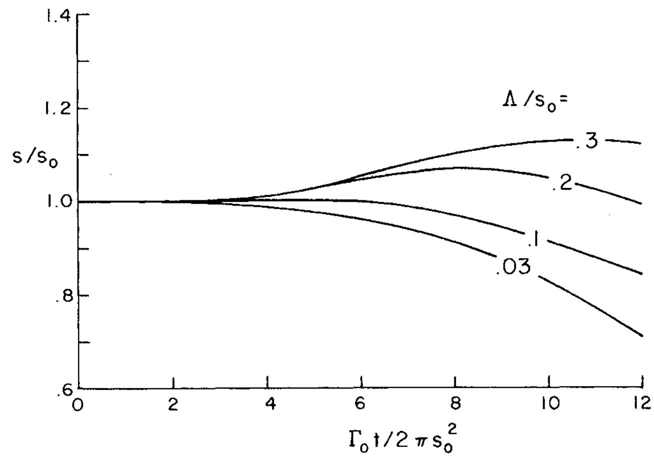

Fig. 14 Calculated vortex semiseparation for four values of the turbulent scale and $\sigma/s_0 = 0.5$, $Fr = 6.0$.

transport correlations can track their equilibrium value, and by neglecting turbulent diffusion. The local energy dissipation rate ϵ is proportional to q^3/Λ, and in turn, using the superequilibrium result, to Λ^2/σ^3. Thus the total descent of a vortex pair with a smaller core, and consequently more kinetic energy, may be less than one with smaller initial energy, due to a more rapid transformation of mean kinetic energy to turbulence, which is in turn dissipated faster. This leaves progressively less mean kinetic energy to be transformed into the potential energy of buoyancy, resulting in decreased total descent. The result of increasing scale is similar in its effect.

V. Conclusions

In this study, we have closely simulated the behavior of a turbulent vortex descending in a stable density stratification, showing agreement between the calculated and observed behavior.

We find a very strong, tight vortex which decays slowly during descent, and which has appreciable circulation after descent has stopped. The core vorticity structure remains well ordered throughout most of the descent, as the vorticity within the core is slowly diffused outward due to a ring of turbulence surrounding the core. A portion of the vorticity diffused away from the core is annihilated by countersign vorticity generated at the boundary of the recirculation cell. The countersign vorticity remains small, less than 1% of the magnitude of the maximum core vorticity, because it is being continually diffused into the cell or swept out of the vicinity of the cell by descent. Although the level of the countersign vorticity is small, the area of the wake containing it reaches an area comparable with that of the recirculation cell. The centroid of the countersign vorticity is primarily above and outboard of the cores. This will tend to drive the cores together, but the net effect of the strength and location of the countersign vorticity with respect to the cores is to halt descent. The circulation of the countersign vorticity reaches a magnitude of nearly 50% of the circulation of the initial primary vorticity, while the primary vorticity is reduced by only about 20% below its initial value at the end of descent. The core circulation remains high and a vortex pair cannot be assumed to have dissipated when it stops descending.

The turbulence near the center of the core is suppressed due to the stability of the flow in this region, and remains small over the descent time of the pair. It reaches a level of only 10% of the peak value outside the core, explaining the persistence of the vortices. However, the rate of annihilation of vorticity, and the extent and strength of the countersign vorticity, are direct consequences of the turbulent diffusion process.

The effect of stable atmospheric stratification, then, is found to halt descent, but not necessarily to completely disorganize the vortex pair.

The effect of decreasing core size for all other parameters equal is to increase the initial energy and the production and dissipation rate of turbulence. It would appear that decreasing the core size for a given scale would decrease the total descent, but this conclusion must be qualified since only one calculation was made for the small core, using one value of the scale. It was also found that increasing the scale for the large core decreases the total descent. This underscores the importance of gaining additional understanding of the turbulent scale length associated with vortices in a stratified atmosphere.

Acknowledgment

The simulation of flight measurements reported here was supported by the U. S. Dept. of Transportation Systems Center under Contract DOT-TSC-1488.

References

[1]Scorer, R. S. and Davenport, L. J., "Contrails and Aircraft Downwash," *Journal of Fluid Mechanics*, Vol. 43, Pt. 3, 1970, pp. 451-464.

[2]Tombach, I. H., "Transport of a Vortex Wake in a Stably Stratified Atmosphere," *Aircraft Wake Turbulence and Its Detection*, edited by H. J. Olsen, A. Goldburg, and M. Rogers, Plenum Press, New York, 1971, pp. 41-57.

[3]Turner, J. S., "A Comparison Between Buoyant Vortex Rings and Vortex Pairs," *Journal of Fluid Mechanics*, Vol. 7, Pt. 3, 1960, pp. 419-432.

[4]Costen, R. C., "Drift of Buoyant Wing-Tip Vortices," *Journal of Aircraft*, Vol. 9, June 1972, pp. 406-412.

[5]Tulin, M. P. and Schwartz, J., "The Motion of Turbulent Vortex Pairs in Homogeneous and Density Stratified Media," Hydronautics, Inc. Technical Rept. No. 231-15, AD 723-184, 1971.

[6]Saffman, P. G., "The Motion of a Vortex Pair in a Stratified Atmosphere," *Studies in Applied Mathematics*, Vol. LI, No. 2, June 1972, pp. 107-119.

[7]Kuhn, G. D. and Nielsen, J. N., "Analytical Studies of Aircraft Trailing Vortices," AIAA Paper 72-42, June 1972.

[8]Crow, S. C., "Motion of a Vortex Pair in a Stably Stratified Fluid," Poseidon Research Rept. No. 1, May 1974.

[9]Narain, J. P. and Uberoi, M. S., "The Motion of a Trailing Vortex Wake in a Stratified Medium," *Atmospheric Environment*, Vol. 8, 1974, pp. 459-473.

[10]Hill, F. M., "A Numerical Study of the Descent of a Vortex Pair in a Stably Stratified Atmosphere," *Journal of Fluid Mechanics*, Vol. 71, Pt. 1, 1975, pp. 1-13.

[11]Hecht, A. M., Bilanin, A. J., Hirsh, J. E., and Snedeker, R. S., "Turbulent Vortices in Stratified Fluids," *AIAA Journal*, Vol. 18, July 1980, pp. 738-746.

[12]Burnham, D. C., Hallock, J. N., Tombach, I. H., Brashears, M. R., and Barber, M. R., "Ground-Based Measurements of a B-747 Aircraft in Various Configurations," U. S. Dept. of Transportation Rept. FAA-RD-78-146, Dec. 1978.

[13]Donaldson, C duP. and Bilanin, A. J., "Vortex Wakes of Conventional Aircraft," AGARDograph AGARD-AG-204, May 1975.

[14]Crow, S. C., "Stability Theory for a Pair of Trailing Vortices," *AIAA Journal*, Vol. 8, Dec. 1970, pp. 2172-2179.

[15]Tombach, I., "Observation of Atmospheric Effects on Vortex Wake Behavior," *Journal of Aircraft*, Vol. 10, Nov. 1973, pp. 641-647.

[16]Hecht, A. M., Bilanin, A. J., and Hirsh, J. E., "Turbulent Line Vortices in Stratified Fluids," AIAA Paper No. 80-0009, Pasadena, Calif., Jan. 1980.

[17]Donaldson, C duP., "Atmospheric Turbulence and the Dispersal of Atmospheric Pollutants," *Proceedings of the Workshop on Micrometeorology*, edited by D. A. Haugen, American Meteorological Society, Science Press, 1973, pp. 313-390.

[18]Lewellen, W. S. and Teske, M. E., "Turbulence Modeling and Its Application to Atmospheric Diffusion," EPA-600/4-75-016b, 1976.

[19]Hecht, A. M., Bilanin, A. J., Hirsh, J. E. and Snedecker, R. S., "Investigation of Stable Atmospheric Stratification Effect on the Dynamics of Descending Vortex Pairs," U.S. Dept. of Transportation Rept. No. FAA-RD-79-10, Feb. 1979.